On the Time of Emergence of Tropical Width Change⊘

Xiao-Wei Quan

*NOAA/Earth System Research Laboratory, and Cooperative Institute for Research in Environmental Sciences,
University of Colorado Boulder, Boulder, Colorado*

Martin P. Hoerling

NOAA/Earth System Research Laboratory, Boulder, Colorado

Judith Perlwitz

*NOAA/Earth System Research Laboratory, and Cooperative Institute for Research in Environmental Sciences,
University of Colorado Boulder, Boulder, Colorado*

Henry F. Diaz

Department of Geography, University of Hawai'i at Mānoa, Honolulu, Hawaii

ABSTRACT

The tropical belt is expected to expand in response to global warming, although most of the observed tropical widening since 1980, especially in the Northern Hemisphere, is believed to have mainly originated from natural variability. The view is of a small global warming signal relative to natural variability. Here we focus on the question whether and, if so when, the anthropogenic signal of tropical widening will become detectable. Analysis of two large ensemble climate simulations reveals that the forced signal of tropical width is strongly constrained by the forced signal of global mean temperature. Under a representative concentration pathway 8.5 (RCP8.5) emissions scenario, the aggregate of the two models indicates a regression of about 0.5° lat °C^{-1} during 1980–2080. The models also reveal that interannual variability in tropical width, a measure of noise used herein, is insensitive to global warming. Reanalysis data are therefore used to constrain the interannual variability, whose magnitude is estimated to be 1.1° latitude. Defining the time of emergence (ToE) for tropical width change as the first year (post-1980) when the forced signal exceeds the magnitude of interannual variability, the multimodel simulations of CMIP5 are used to estimate ToE and its confidence interval. The aforementioned strong constraint between the signal of tropical width change and global mean temperature change motivates using CMIP5-simulated global mean temperature changes to infer ToE. Our best estimate for the probable year for ToE, under an RCP8.5 emissions scenario, is 2058 with 10th–90th percentile confidence of 2047–68. Various sources of uncertainty in estimating the ToE are discussed.

1. Introduction

There is medium to high confidence that the tropics have expanded since about 1980, with an estimated 70–200-mi poleward shift (1 mi ≈ 1.61 km) occurring in each hemisphere (Wuebbles et al. 2017). While most metrics used to define the tropical edge indicated an expansion, uncertainties exist principally with regard to the rate of tropical expansion during the recent 30-yr record, with different magnitudes found among various datasets and metrics of the tropical edge (e.g., Davis and Rosenlof 2012; Quan et al. 2014; Lucas et al. 2014).

Notwithstanding the uncertainty in how much the tropics have actually expanded, model-based investigations have explored whether the tropical widening since about 1980 is symptomatic of a warming world (e.g., Lu et al. 2007). Results from historical simulations

of phases 3 and 5 of the Coupled Model Intercomparison Project (CMIP) show a comparatively smaller rate of expansion associated with anthropogenic climate change than the magnitude of change observed (e.g., Johanson and Fu 2009; Hu et al. 2013; Vallis et al. 2015). It is therefore unlikely that most or even a substantial fraction of the observed tropical expansion of recent decades has resulted from human-induced climate change (e.g., Quan et al. 2014; Garfinkel et al. 2015; Allen and Kovilakam 2017). Internal atmospheric variability and decadal tropical SST variability related to El Niño–Southern Oscillation (ENSO) can explain discrepancies in magnitudes between the strong observed tropical expansion of recent decades and the weaker anthropogenic change–induced expansion in coupled model simulations (Garfinkel et al. 2015; Allen and Kovilakam 2017).

The current study seeks to understand when the climate change signal of tropical edge change is likely to emerge relative to the magnitude of interannual variability (herein defined to be the noise) in annual tropical width. We specifically inquire when an altered location of the tropical edge due to anthropogenic forcing becomes sufficiently prominent so as to mark, at least conceptually, the dawn of an altered climate state concerning tropical extent.

We apply formal time of emergence (ToE) analysis methods (following Hawkins and Sutton 2012) to estimate when a tropical width change will be detectable. The method of ToE has been applied to studies of change in a wide variety of geophysical conditions including droughts (e.g., Orlowsky and Seneviratne 2013), catchment hydrology (Addor et al. 2014), regional sea level (Lyu et al. 2015), ocean biogeochemistry (Keller et al. 2014), daily temperature extremes (Scherer and Diffenbaugh 2014; Harrington et al. 2016), and regional temperature and precipitation change (Lehner et al. 2017) to name a few. This is the first study to apply such formal methods in estimating the likely date of Hadley cell widening. We use a late twentieth-century period as a reference for emergent change in order to align with many previous studies on the Hadley cell that employed 1980 as the beginning point of tropical widening (e.g., Hu and Fu 2007; Seidel and Randel 2007; Johanson and Fu 2009; Birner 2010; Davis and Rosenlof 2012; Quan et al. 2014; Allen and Kovilakam 2017), motivated in large part by the availability of modern reanalyses that make diagnosis of factors determining variability in tropical width feasible. It should be recognized, however, that the ToE will be different if using an earlier reference period. Indeed, it is possible that inception of an altered tropical belt may have already occurred when viewed from a preindustrial era reference, but the late

twentieth century is arguably a more relevant reference to employ from an adaptation perspective of current society. Owing to observational limitations, empirical estimates of the ToE based on changes relative to periods appreciably preceding the modern reanalysis period are not expected to be reliable.

To estimate the ToE of the climate change–induced tropical expansion we use a variety of coupled ocean–atmospheric model simulations. As described further in section 2, these include two large ensembles of coupled ocean–atmosphere model experiments and an ensemble of single runs of the multimodel experiments from CMIP5 (Taylor et al. 2012). Analogous to Hawkins and Sutton (2012), the ToE is defined as the first year in which the magnitude of anthropogenically forced change in the tropical edge exceeds the magnitude of interannual variability. Section 3 presents an analysis of tropical widening occurring in the two large ensembles and explores especially the relationship between the rate of tropical expansion and the rate of global mean temperature rise. Section 4 calculates the probable ToE for the human-induced signal of tropical widening using the multimodel CMIP5 simulations. Drawing on the relation between the forced signal in tropical width and the forced signal of global mean temperature derived from the large ensemble experiments and using observational data to constrain the magnitude of interannual variability, the probable year of emergence and its 10th–90th percentile confidence interval is derived. A summary and discussion are provided in section 5.

2. Data and method

a. Observations

Reanalysis products are used to describe variability in tropical width during 1980–2016, including ERA-Interim (Dee et al. 2011), JRA-55 (Kobayashi et al. 2015), MERRA (Rienecker et al. 2011), and MERRA-2 (Gelaro et al. 2017). Two indicators for the location of the tropical width are diagnosed for annual mean conditions. One is the poleward-most latitude at which zonally averaged precipitation P equals zonally averaged evaporation E, and the other is the zero-crossing latitude of the zonal-mean meridional streamfunction at 500 hPa Ψ_{500}. Results based on those two indicators are intercompared, and we note that Davis and Birner (2017) found very similar CMIP5-projected tropical belt trends when using the zero-crossing latitudes of Ψ_{500} and vertically averaged Ψ, respectively. The numerical method for calculating these from the reanalyses is described in Davis and Rosenlof (2012), and the annually averaged mass streamfunction is calculated using the

annual averaged wind fields. Figure 1 of Quan et al. (2014) provides a schematic of the spatial relation of each indicator with various climatological features of the zonally averaged climate.

Observed global mean surface temperature is derived from the Goddard Institute for Space Studies (GISS) Surface Temperature Analysis (GISTEMP; GISTEMP Team 2016; Hansen et al. 2010), whereas sea surface temperature diagnosis is derived from the Hurrell et al. (2008) analysis.

b. Coupled climate model simulations

Two large ensemble coupled ocean–atmosphere model simulations are diagnosed. The NCAR Community Earth System Model Large Ensemble (CESM-LE; Kay et al. 2015) consists of 40 members spanning 1920–2100. The atmospheric component of CESM-LE [Community Atmosphere Model, version 5 (CAM5)] employs a finite-volume scheme for its dynamical core with spatial resolution of $0.9° \times 1.25°$ and 30 vertical levels from surface to near 3 hPa. Time-evolving specified radiative forcings include greenhouse gases [e.g., CO_2, CH_4, NO_2, O_3, and chlorofluorocarbons (CFCs)], aerosols, and solar and volcanic aerosols. External forcing after 2005 follows a representative concentration pathway 8.5 (RCP8.5) protocol. The Second Generation Canadian Earth System Model (CanESM2; Arora et al. 2011; Sigmond and Fyfe 2016; Kushner et al. 2018) consists of a 50-member ensemble spanning 1950–2100. The atmospheric component of CanESM2 [Fourth Generation Canadian Atmospheric General Circulation Model (CanAM4)] is a spectral model employing spectral T63, triangular truncation at wavenumber 63 ($\sim$2.8° latitude–longitude), spatial resolution, and 35 vertical levels from the surface to 1 hPa. Natural and historical forcing in the CanESM2 experiments for 1950–2005 include variability in greenhouse gases, tropospheric and stratospheric aerosols, ozone, land use, and solar variability, while an RCP8.5 protocol is used for radiative forcing after 2005 as in the CESM simulations.

To increase the sample of model configurations, we also use data from the first member of each of 35 different models contributing to CMIP5 experiments. This ensemble of multiple models includes single runs of CanESM2 and CESM-LE. Each member of these transient coupled model runs is subject to the same radiative forcing as the large ensemble coupled model simulations with historical forcing prior to 2005 and an RCP8.5 scenario thereafter.

The forcings used in the experiments studied herein follow the CMIP5 protocol (http://cmip-pcmdi.llnl.gov/cmip5/forcing.html), although there are some differences in treatments (e.g., specifying emissions rather than concentrations for some chemical species in Earth system models). Ozone forcing as used in the CMIP5 models is described in Eyring et al. (2013). For CanESM2, two additional 50-member ensemble simulations are examined in which single forcings are applied involving stratospheric ozone only and anthropogenic aerosols only, respectively [for further details of these experiments see Gillett et al. (2013) and Banerjee et al. (2017)].

c. Time of emergence

We define ToE for tropical width change as the year when the signal S of forced change in tropical width first exceeds the magnitude of noise N. The approach is analogous to Hawkins and Sutton (2012), with the principal difference being that noise against which the forced signal is compared is derived from statistics of *total* interannual variability, rather than from an estimate of the *internal component* of the variability such as might be based on the calculation of interannual variability relative to a detrended time series or from an independent set of preindustrial control experiments. The N as computed herein is thus a combination of internal and external components of the interannual variability. The main reason for using the total interannual variability for describing N rather than the internal component alone is that only the former can be estimated from observations, and thus only the former can be used to constrain the models. Section 4 addresses observational constraints on total interannual variability of tropical width and reveals that the total interannual variability is roughly 5% greater than the internal component alone (as estimated from the large ensemble simulations). As such, results for estimating the ToE are not particularly affected by the aforementioned options in defining N.

Uncertainties in the ToE can be estimated by various methods. For example, comparing values based on $S/N > 1$ versus $S/N > 2$, comparing ToE derived from our two different large ensemble simulations, comparing the statistics of ToE estimated from the multimodel ensemble of CMIP5 simulations, and/or by comparing ToE derived from different RCP assumptions for future climate change.

To diagnose the magnitude of time-varying forced signals in our two large ensembles, the method of Liebmann et al. (2010) is used, which involves constructing two-dimensional parameter diagrams. To illustrate, Fig. 1 shows such a diagram for time-varying trends of annually averaged global mean surface temperature (GMST) during 1950–2017. Every possible trend (having at least a 10-yr duration) is calculated using linear regression by least squares fit. Columns in
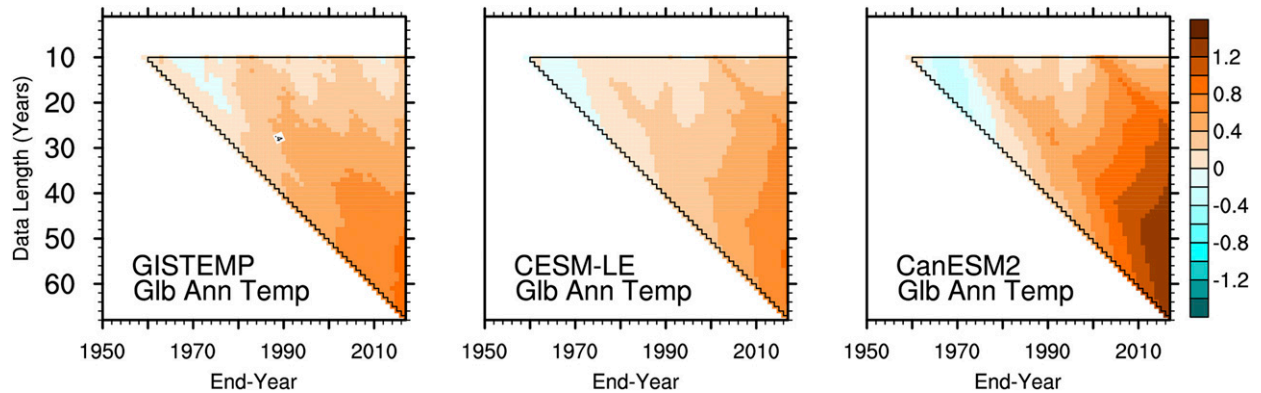
FIG. 1. Changes in annually averaged GMST (°C) based on linear trend calculation as a function of length of time segment and end year for the period 1950–2017. Shown are values for observations (left) GISTEMP and large ensemble climate simulations of (center) CESM-LE and (right) CanESM2. Changes calculated for individual ensemble members are averaged for center and right panels.

the parameter diagram display trends over various lengths for a fixed end year—all trends ending in 2017 are plotted at the far right in each panel of Fig. 1. Rows in the parameter diagram display trends of a fixed length for various end years—all 10-yr duration trends for end years ranging from 1959 to 2017 are plotted at the top in each panel of Fig. 1. The plotted values are the temperature trend (°C yr^{-1}) multiplied by the length of segment, with the longest duration trend (67 yr) plotted in the bottom right of the parameter diagram. Figure 1 reveals the well-known observed global warming (Fig. 1, left), with a total increase since 1950 (ending in 2017) of about 0.9°C. The trends in ensemble means of the two experiments also reveal warming, with the 1950–2017 temperature increase being slightly less than observed in CESM-LE (0.8°C; Fig. 1, center) and considerably greater than observed in CanESM2 (1.3°C; Fig. 1, right).

3. ToE of tropical width change in two large ensemble simulations

Tropical width trends using the mass streamfunction metric are shown in Fig. 2 for CESM-LE and CanESM2. The two-dimensional parameter diagrams (Fig. 2, top) show a tropical widening for all trend segments beginning in 1980 (hypotenuse). A progressively greater widening for longer periods is indicative of a quasi-linear scaling of tropical width change with global warming, as will be discussed further in section 4. For 1980–2017, CESM-LE total tropical widening is approximately 0.5° latitude compared to almost double that occurring in CanESM2, in line with the simulated approximately 0.8°C global warming in CESM-LE compared to approximately 1.3°C warming in CanESM2 (see Fig. 1). Indeed, when evaluated with the simulated noise in each model, the externally forced signal begins

exceeding the noise (one standardized departure of interannual variability) at about 2020 in CanESM2, whereas the signal does not emerge from the noise until about 2060 for CESM-LE (see hatching in Fig. 2, top).

Shown in the middle and bottom panels of Fig. 2 are time series of total tropical width for each ensemble member (solid gray) of CESM-LE and CanESM2. Their time evolution is compared to a mean tropical width (solid black) and the plus one standard deviation of interannual variability (dashed blue), each derived using a 1980–2010 reference period. Box-and-whisker plots are shown at 10-yr intervals in order to summarize the statistics of trends for progressively later end years, all relative to a 1980 beginning. The two factors that determine time of emergence are evident in these plots, both of which differ between the models. First, as already evident from the two-dimensional parameter diagrams, the magnitude of forced change in tropical width is greater in CanESM2 compared to CESM-LE. Second, the magnitude of interannual variability is less in CanESM2 (0.8° latitude) compared to CESM-LE (1.2° latitude). These differences each serve to accelerate the ToE in CanESM2 relative to CESM-LE.

These principal findings concerning ToE using a mass streamfunction metric for tropical width are largely reproduced using a $P - E = 0$ latitude crossing analysis. Results from the latter, shown in Fig. 3, again demonstrate a progressive tropical widening with time, but with a much earlier ToE in CanESM2 compared to CESM-LE simulations. We find significant correlation between trends in tropical width based on the two indices (see Fig. S1 in the supplemental material), with a somewhat stronger relationship between them in CanESM2 than in CESM1. The agreement in tropical width trends calculated using these two indices is similar to that
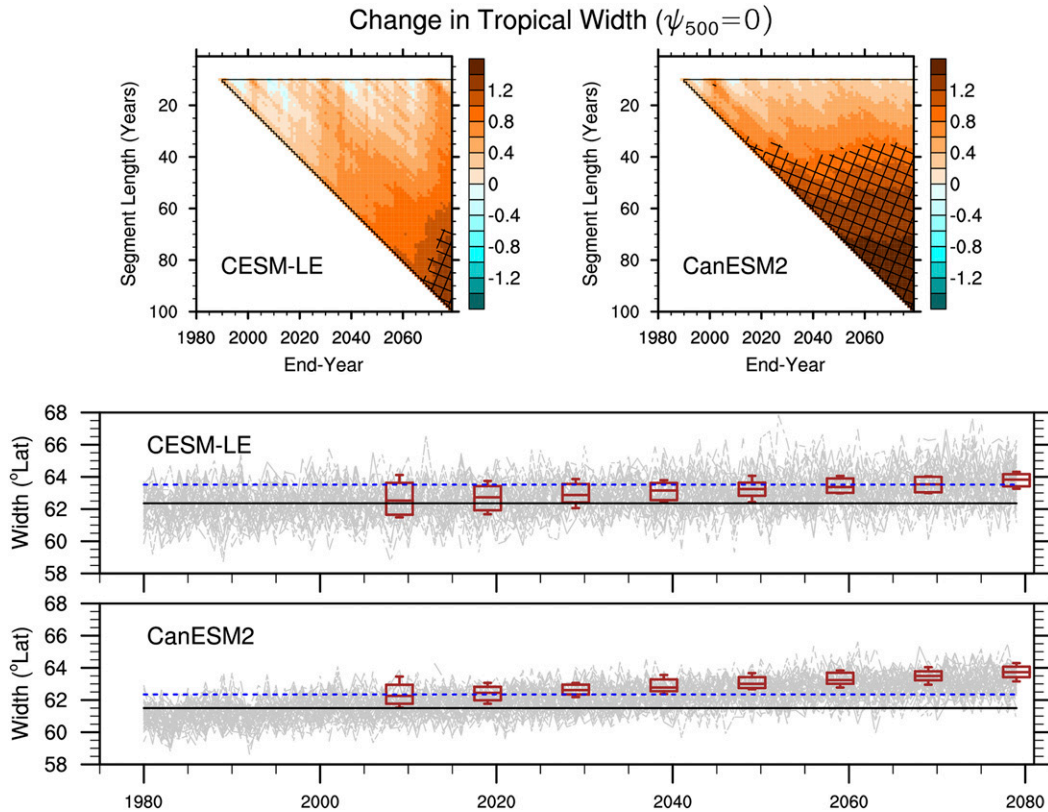
FIG. 2. (top) Changes in annually averaged tropical width (° lat) based on linear trend calculations as a function of length of time segment and end year for the period 1980–2080. Shown are average values for large ensemble climate simulations of (left) CESM-LE and (right) CanESM2. Hatched areas indicate values that are larger than ensemble-averaged std dev calculated over the period 1980–2010. (middle),(bottom) Simulated temporal evolutions of the annual-mean tropical width from 1980 to 2080. Gray lines indicate time series of all ensemble members for (middle) CESM-LE and (bottom) CanESM2. The long horizontal solid line in each plot shows the 1980–2010 mean tropical width value. The long horizontal dashed blue line in each plot indicates ensemble mean plus one 1980–2010 std dev, which is the same value used in the top panels for hatching. Box-and-whisker plots (in red) illustrate changes to date above the 1980–2010 mean of the model ensemble that are calculated based on trend analysis for all segments beginning in 1980. Solid lines represent ensemble mean, and boxes and whiskers represent 10% and 90% ranks and max and min change values, respectively.

found among the same indices in Quan et al. (2014) but based on a different coupled model, and is also similar to the relationship between a mass streamfunction indicator and the latitude of the maximum surface westerlies as examined in Vallis et al. (2015). In the subsequent analysis of section 4 where observational data are used to constrain tropical width variability and multimodel CMIP5 experiments are introduced, the mass streamfunction index of tropical width is used.

4. Constraining the ToE

The CanESM2 and CESM-LE experiments yield significantly different ToE for the tropical widening signal. Availability of large ensembles for both models reveals that the differences are structural rather than

due to sampling. These structural differences arise from two conflating factors: 1) a stronger signal (larger S) of forced tropical widening, and 2) a weaker magnitude for interannual variability (smaller N) of the tropical belt in CanESM2 versus CESM-LE. The ToE therefore occurs roughly 40 years earlier in CanESM2, prompting the questions which (if any) of the two estimates is more realistic, and whether the difference between them reasonably measures the uncertainty in ToE.

Taking further advantage of the large ensembles, we explore constraints that might be applied to ToE in order to reduce, or at least better quantify, the uncertainty in its estimate. Concerning the first factor, we examine in Fig. 4 the statistical linkages between dynamic and thermodynamic responses to external radiative forcing. Shown are scatterplots of the ensemble-averaged
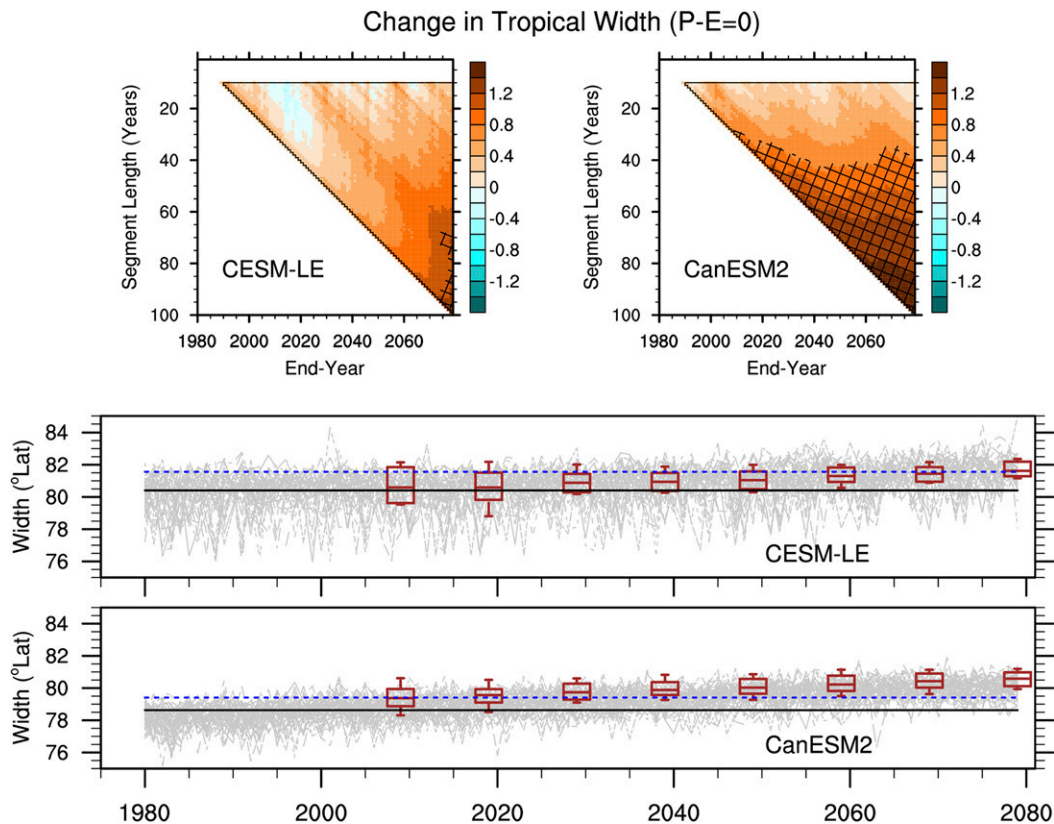
Change in Tropical Width (P−E=0)

FIG. 3. As in Fig. 2, but the tropical width is determined from the $P - E = 0$ metric of tropical width.

tropical width versus global mean surface temperature using annual data from 1980–2080. Both models exhibit similar and strong relationships between low-frequency variations in their signals of tropical width and GMST with correlations of about 0.9 (see also Amaya et al. 2018). The regression relationships between tropical width and GMST during 1980–2080 as a whole are also similar, though not identical for the two models. The values of 0.42° and 0.55° lat °C^{-1} in CESM-LE and CanESM2, respectively, indicate tropical width change to be strongly constrained by global surface temperature change. The two values are within the range of prior estimates of the rate of annual-mean Hadley cell widening as a function of GMST. For instance, a 0.45° lat °C^{-1} sensitivity is found in climate simulations spanning the Last Glacial Maximum to the end of the twenty-first century (Son et al. 2018), a 0.6° lat °C^{-1} sensitivity occurs in an idealized general circulation model (Frierson et al. 2007), and the synthesis of CMIP5 projections in Vallis et al. (2015) indicate about 0.5° lat °C^{-1}.

A cautionary point is that Vallis et al.'s (2015) analysis of single runs from different CMIP5 models found that the magnitude of Hadley cell expansion was not well correlated with the magnitude of GMST responses (see

their Fig. 21). Their results imply that GMST does not serve as a strong constraint on tropical width, at least when viewed across models. However, our results reveal considerable sampling noise in tropical width trends
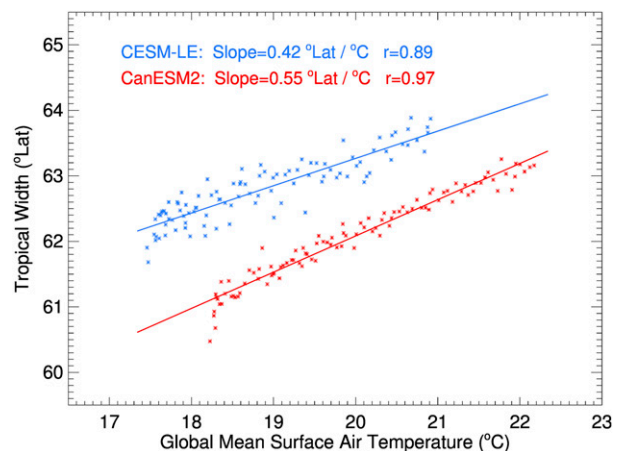

FIG. 4. Simulated annually averaged tropical width values as a function of GMST for the period 1980–2080. Shown are ensemble-mean values for each year (dots) together with respective regression line for CESM-LE (blue) and CanESM2 (red).

1980-2010 Standard Deviation of Tropical Width

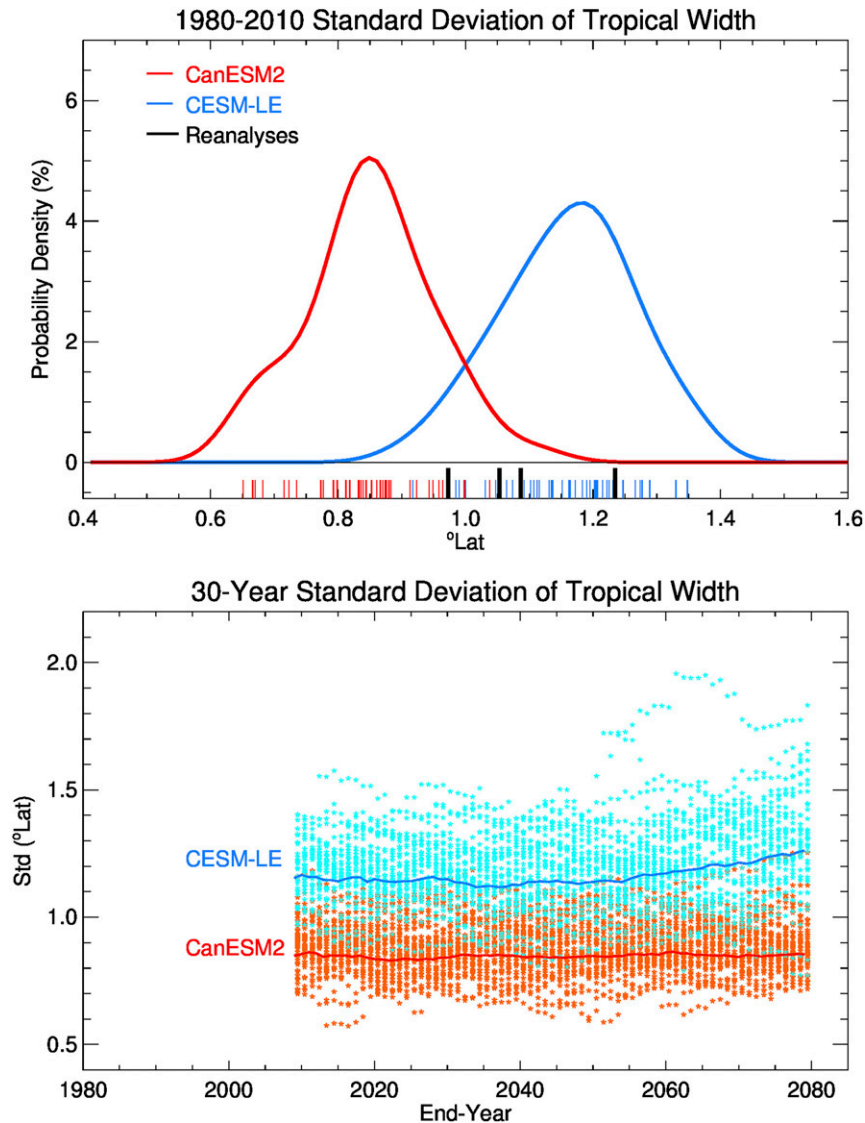

30-Year Standard Deviation of Tropical Width

FIG. 5. (top) PDF determined from ensemble values of 1980–2010 std dev of annual-mean tropical width in CanESM2 (red) and CESM-LE (blue). Red and blue ticks at bottom represent individual model ensemble members. The four black ticks represent reanalysis values. (bottom) Standard deviations of annual-mean tropical width for moving 30-yr windows calculated over the 1980–2080 period for two large model ensembles. For CESM-LE, light blue asterisks show values for each individual run, and the blue line shows the average of the ensemble member values in each 30-yr window. Corresponding values for CanESM2 are shown in orange and red.

among single runs of the large ensemble experiments derived from the same model (see Fig. 2). It is thus possible that the scatter relation of trends from single runs of multiple models may be unrepresentative of forced signal sensitivities. As supporting evidence, we find little correlation between Hadley cell expansion versus GMST change [for the 70-yr period 2006–75 examined in Vallis et al. (2015)] when using individual members of our large ensemble simulations (Fig. S2 in the supplemental material). We reconcile this finding

(and also reconcile the Vallis et al. finding) with the contrary indication for a strong constraint based on the ensemble-mean diagnosis (Fig. 4) by invoking the overwhelming influence of sampling noise on tropical width variability among individual runs.

Concerning the second factor in which the magnitude of interannual variability of the tropical belt in CanESM2 is about 30% weaker than in CESM-LE, we use reanalysis products to estimate the observed interannual variability of tropical width. Figure 5 (top)

compares 4 different reanalysis products (black tick marks) against the statistics of interannual variability in CESM-LE (PDF in blue) and CanESM2 (PDF in red) during 1980–2010. It is evident that the reanalyses are in overall better agreement with CESM-LE statistics and that the CanESM2 interannual variability in tropical width is almost certainly too weak (which contributes to a premature ToE). We further find this measure of noise to be largely insensitive to radiative forcing during 1980–2080 as revealed by the absence of meaningful trends in the time series of 30-yr moving interannual variability (Fig. 5, bottom). This result provides justification for using reanalysis products of the recent observational record to constrain the magnitude of interannual variability simulated in the models. The four estimates range from 0.97° to 1.23° latitude, and here we use their simple average (1.09° latitude). By comparison, the magnitude of interannual variability in tropical width is 1.15° and 0.85° latitude in CESM-LE and CanESM2, respectively, during 1980–2010. In the case of the large ensemble simulations, we also estimate the internal component of the interannual variability, whose values are 1.14° and 0.80° latitude in CESM-LE and CanESM2, respectively, during 1980–2010. Thus, most of the total variability in the interannual location of tropical edges is due to internal noise of the coupled ocean–atmosphere system. The imposed observational constraint on total variability is thereby not materially different from constraining the internal component alone (though the internal component cannot be readily derived from the observational data).

To summarize, the results lead to the following assumptions regarding constraints on the ToE: The signal of tropical width change scales with the magnitude of global warming at a rate 0.49° lat $°C^{-1}$ and the noise based on the magnitude of total interannual variability is 1.09° latitude. Thus, for a signal-to-noise ratio larger than one ($S/N > 1$), the ToE would correspond to the first year when the anthropogenically forced GMST signal exceeds 2.2°C (above a 1980 reference). Note that using N based on the magnitude of the internal variability component only slightly changes the required GMST threshold (by less than 5% to ~2.1°C in our analysis of the CESM-LE and CanESM2 models). Figure 6 shows times series of GMST for each member of CanESM2 (Fig. 6, top), each member of CESM-LE (Fig. 6, middle), and each single run of the 35 different CMIP5 model (Fig. 6, bottom). Gray bands illustrate the span of time between the first member of the ensemble exceeding 2.2°C and the last member exceeding 2.2°C.

The results shown in Fig. 7 are then the outcome of translating the model temperature trend information into equivalent ToE under the aforementioned assumptions. Shown are PDFs for the three different ensembles: CanESM2 (red), CESM-LE (blue), and CMIP5 (black). Thick tick marks indicate the mean ToE for each distribution, and the corresponding thin tick marks show the 10th- and 90th-percentile ranges. It is evident that CanESM2's ToE is an extreme early occurrence relative to the multimodel statistics, whose mean value is outside the 10th percentile of CMIP5 statistics. This much earlier ToE is a consequence of its larger projected warming magnitude. Note that had the bias in the noise component of CanESM2's tropical belt variability not been constrained as per observations, the ToE would have been an additional quarter century earlier. By contrast, and perhaps coincidentally, the ToE estimated from the CESM-LE is nearly identical to the mean estimate derived from the CMIP5 ensemble. This is perhaps unexpected since the CESM1 transient climate response (TCR) of 2.33°C is on the higher end of the very likely range of roughly 1°–3°C based on models contributing to the IPCC Fourth Assessment Report (IPCC 2013).

The statistics of ToE based on the multimodel CMIP5 ensemble (Fig. 7, PDF in black) indicates the most likely ToE is near about 2058, with 10th and 90th percentiles of 2047 and 2068, respectively. It is evident that the spread of this distribution is principally a consequence of different GMST sensitivities of the individual models rather than due to sampling noise. This is clearly illustrated by the fact that the mean ToE for the two large ensembles differs more from each other than the spread of each PDF associated with internal variability alone. Given that the extent of the tropical belt is strongly constrained by GMST, and given a temporally invariant noise of Hadley cell variability, it follows that the uncertainty in the ToE estimated here must principally reflect uncertainty in TCR. This would be true whether ToE is based on a threshold exceedance of $S/N > 1$ or $S/N > 2$. For the latter higher threshold, GMST would need to eclipse 4.4°C, and there are few if any model simulations among any of the ensembles studied herein that achieve such warming before 2080 under the RCP8.5 scenario (see Fig. 6). Thus, our results indicate that ToE for tropical width change would occur after 2080 for the more stringent detectability requirement $S/N > 2$.

Finally, it is worth noting some implications of different RCP scenarios for ToE. Under RCP2.6 emissions, GMST do not exceed the 2.2°C threshold (relative to a 1980 reference) throughout the integrations of the twenty-first century (IPCC 2013), indicating the tropical belt would be unlikely to change beyond the typical
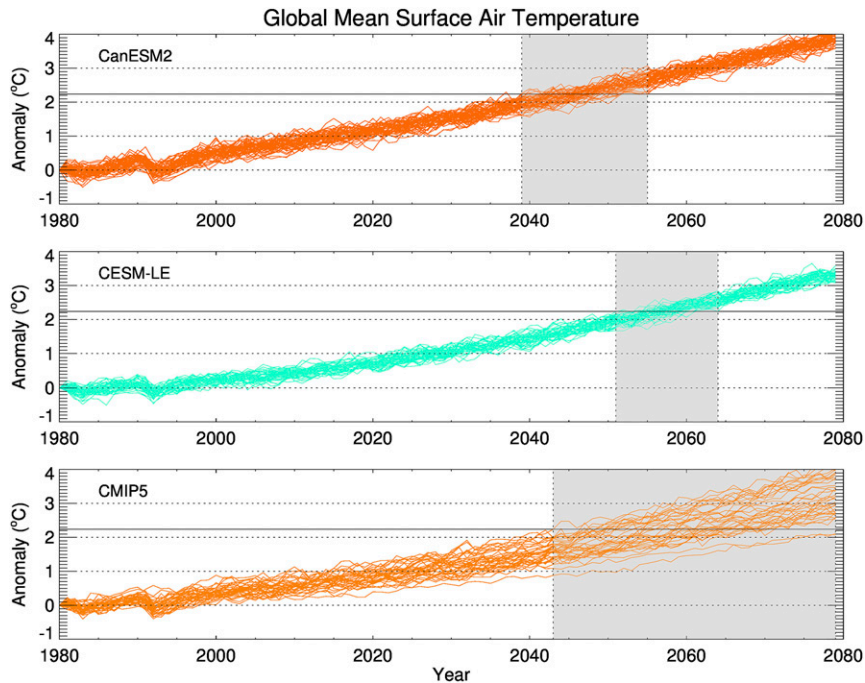
FIG. 6. Changes in annually averaged GMST values in (top) CanESM2, (middle) CESM-LE, and (bottom) the 36 climate models of CMIP5. The changes are relative to the annual-mean value of 1980 for each of the individual runs. Shaded gray areas indicate the range of ToE for which changes in the GMST begins to exceed 2.2°C indicated by the thin black horizontal line in each panel (see text for further explanations).

range of interannual variability. For an RCP6.0 scenario, sufficient warming occurs in projections for the latter half of the twenty-first century (IPCC 2013) to also yield an emergent tropical widening signal (for $S/N > 1$) but delayed by approximately a quarter century to roughly 2080.

5. Summary and discussion

a. Summary

The time of emergence (ToE) of the human-induced signal of tropical belt widening has been estimated using large ensemble climate simulations together with historical observations to constrain model projections. We applied formal methods of ToE analysis to suites of large ensemble climate simulations and provided, for the first time, an estimate of the likely date when tropical width change will become detectable. We defined ToE for tropical width change as the first year (post-1980) when the forced signal S exceeded the magnitude of noise N measured by interannual variability of tropical belt fluctuations. Analysis of two large ensemble climate simulations revealed the forced signal of tropical width to be strongly controlled by the forced signal of global mean temperature. Under an RCP8.5 emissions scenario,

the aggregate of the two models indicated a regression relationship of about 0.5° lat °C^{-1} during 1980–2080 in agreement with several independent estimates of Hadley cell sensitivity to global warming. The large ensemble simulations also revealed that interannual variability in
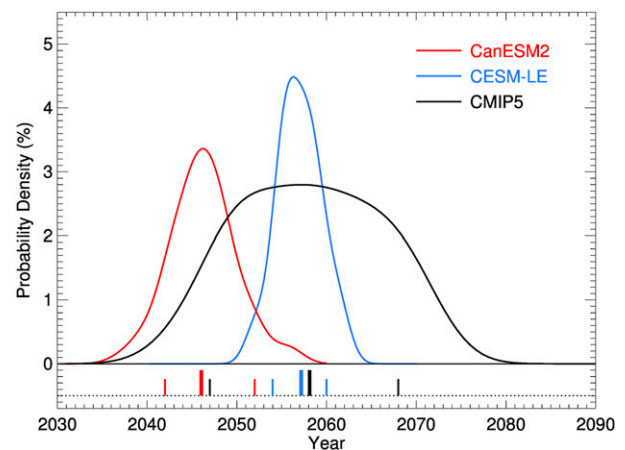

FIG. 7. PDF of estimated ToE based on the projected future changes for CanESM2 (red), CESM-LE (blue), and CMIP5 models (black). For each model ensemble, the long thick vertical ticks at the bottom indicate corresponding ensemble mean, and short thin ticks represent the corresponding 10% and 90% percentile values.

tropical width, a measure of intrinsic noise, is mostly insensitive to global warming. Four different modern reanalysis products were thus used to constrain the noise, whose magnitude was estimated to be 1.09° latitude.

Our best estimate of the probable year for ToE (relative to 1980), under an RCP8.5 emissions scenario and for $S/N > 1$ was 2058, with a 10th–90th percentile confidence range of 2047–68. The results were derived by using the multimodel simulations of CMIP5, convolving each model's projected temperature trend with the aforementioned regression relation, using the observationally derived interannual variability in the tropical belt to constrain the noise, and calculating the equivalent ToE for each model. The CMIP5 multimodel runs were shown to provide a more reliable estimate of the ToE than using large ensembles of single models and also to yield a more representative measure of uncertainty. The uncertainty in ToE of tropical width, for a particular RCP emission scenario, was shown to be determined by the uncertainty in transient climate response (TCR) among CMIP5 models. Given the strong constraint on ToE by the magnitude of global warming, results further indicated that a change in tropical width would emerge about 25 years later (2080) under an RCP6.0 scenario, while no emergent change in the Hadley cell extent would occur in the twenty-first century under an RCP2.6 scenario.

b. Discussion

A source of uncertainty in ToE concerns the sensitivity of the Hadley cell to global mean surface temperature change. While we found the forced signal of tropical width to be strongly constrained by GMST in each of two large ensembles, the regressions differed in magnitude with a 30% greater sensitivity in CanESM2 than CESM-LE. The implied uncertainty in the GMST warming threshold required for detection of tropical width change is thus 2.0° and 2.6°C if using the CanESM2 and CESM-LE regressions, respectively. As such, the most probable year for ToE is 2054 and 2066 based on these two particular values of Hadley cell–GMST relationships. The range between these two estimates, derived from our two large ensemble simulations, is within the sampling range of Hadley cell sensitivity to global temperature found in other studies using different models and forcings. It would be premature to argue that the full range of Hadley cell sensitivities to GMST is currently known. Nonetheless, our results are suggestive that uncertainty in the ToE for tropical width change has two comparable sources: one the uncertainty in magnitude of Hadley cell–GMST relationships and the other uncertainty in GMST sensitivity to greenhouse gas (GHG) forcing.

Until a more robust quantification for the uncertainty in the Hadley cell sensitivity to global warming becomes available, it should be recognized that the 10th–90th percentile range for ToE presented herein is almost certainly too small. For instance, the 10th percentile value for ToE, as an indication for the earliest plausible emergence of a tropical widening signal (under RCP8.5), would be 2043 if using the CanESM2's high sensitivity, and 2054 if using the CESM-LE low sensitivity. Such a difference of about a decade is smaller, however, than those arising from assuming an RCP8.5 versus RCP6.0 scenario, and much smaller than differences from requiring a $S/N > 2$ versus $S/N > 1$. It should also be noted that the ToE for tropical width change may depend on the metric used to define tropical edge location. Although our analysis using a dynamical indicator (Ψ_{500}) yielded similar rates of change to that based on a hydrological indicator ($P - E$) in CanESM2 and CESM-LE, this is not expected to be generally true across all models (Seviour et al. 2018) as different physical factors arise in controlling dynamical versus hydrological-defined tropical edges (e.g., Davis and Birner 2017).

Our best estimate of the ToE (circa 2058) is appreciably later than that implied by Amaya et al. (2018) based on their analysis of a single large model ensemble. Amaya et al. state that a forced signal may already have emerged above the noise in the Southern Hemisphere but may require several more years to emerge in the Northern Hemisphere. Our result indicates that several more decades are likely necessary for the forced signal to emerge above the noise (for the combined NH and SH tropical width). While their approach contrasts in several ways from our method making definitive comparisons difficult, we note that their study focused on a leading internal mode of tropical edge variability using a joint empirical orthogonal function (EOF). This single mode explained only 49% of the total internal variance in their model, and as such a comparison against the forced signal might imply earlier detectability than when considering the full internal variability, as assessed herein.

Concerning the forced signal, our analysis has focused on the so-called all-forcings experiments of the CMIP5 models, leaving open the question as to how much of the time-evolving tropical widening may result from sensitivity to particular forcings. While a comprehensive assessment is beyond this paper's scope, two additional 50-member ensembles of CanESM2 were diagnosed that were subjected to only stratospheric ozone and anthropogenic aerosol variability, respectively. For tropical width trends ($P - E = 0$) during 1980–2020, the effects of these two factors were found to be small (not shown)

when compared to the tropical width change associated with full forcing, indicating the dominant effect of GHG changes in the near term. On the longer 1980–2100 time scale, a weak contraction of the tropical width was found to occur in response to projected stratospheric ozone change. This signal, however, was nearly an order of magnitude weaker than that associated with full forcing in CanESM2, suggesting that the tropical widening projected by the end of the twenty-first century is almost entirely GHG driven. How these results might vary with assumptions on the rate of ozone recovery and also may depend on model sensitivities are each important issues requiring further research before strong conclusions on individual factors can be drawn.

The ToE estimates provided herein pertain to annually averaged conditions. The seasonality has not been explored, though there are indications for seasonality in anthropogenically forced tropical width change (e.g., Kang and Lu 2012; Vallis et al. 2015). Since the noise of intrinsic variability is likely to also vary seasonally, it remains to be determined how much the signal-to-noise ratio (S/N) itself, and hence ToE, varies throughout the year.

Given indications for hemispheric asymmetry in tropical edge sensitivities to external radiative forcing (e.g., Vallis et al. 2015; Amaya et al. 2018; Son et al. 2018), the ToE identified for *total* tropical width in our study may not apply to either the Northern Hemisphere (NH) or Southern Hemisphere (SH) individually. Calculations of annual Hadley cell expansion during 2006–75 within CMIP5 models indicates a stronger poleward expansion in the SH (Vallis et al. 2015). Further, a NH expansion appears less reproducible than a SH expansion among samples of individual model simulations, a distinction that appears to be independent of the nature of external radiative forcing (e.g., Last Glacial Maximum to future climate experiments, transient 1% CO_2 experiments, and CMIP3 and CMIP5 projections). Yet, modeling studies also suggest that the internal noise of NH tropical edge variability may be appreciably greater from that occurring in the SH (Quan et al. 2014). It is thus possible that a less robust signature of the signal in NH tropical width change found in model experiments may be in part due to larger sampling noise, rather than being a symptom of weaker sensitivity alone. The extent to which appreciable differences occur in the ToE for tropical edge change in each hemisphere is thus a question requiring further study.

REFERENCES

Addor, N., O. Rössler, N. Köplin, M. Huss, R. Weingartner, and J. Seibert, 2014: Robust changes and sources of uncertainty in the projected hydrological regimes of Swiss catchments. *Water Resour. Res.*, **50**, 7541–7562, https://doi.org/10.1002/2014WR015549.

Allen, R. J., and M. Kovilakam, 2017: The role of natural climate variability in recent tropical expansion. *J. Climate*, **30**, 6329–6350, https://doi.org/10.1175/JCLI-D-16-0735.1.

Amaya, D. J., N. Siler, S.-P. Xie, and A. J. Miller, 2018: The interplay of internal and forced modes of Hadley cell expansion: Lessons from the global warming hiatus. *Climate Dyn.*, **51**, 305–319, https://doi.org/10.1007/s00382-017-3921-5.

Arora, V. K., and Coauthors, 2011: Carbon emission limits required to satisfy future representative concentration pathways of greenhouse gases. *Geophys. Res. Lett.*, **38**, L05805, https://doi.org/10.1029/2010GL046270.

Banerjee, A., L. M. Polvani, and J. C. Fyfe, 2017: The United States "warming hole": Quantifying the forced aerosol response given large internal variability. *Geophys. Res. Lett.*, **44**, 1928–1937, https://doi.org/10.1002/2016GL071567.

Birner, T., 2010: Residual circulation and tropopause structure. *J. Atmos. Sci.*, **67**, 2582–2600, https://doi.org/10.1175/2010JAS3287.1.

Davis, N., and T. Birner, 2017: On the discrepancies in tropical belt expansion between reanalyses and climate models and among tropical belt width metrics. *J. Climate*, **30**, 1211–1231, https://doi.org/10.1175/JCLI-D-16-0371.1.

Davis, S. M., and K. H. Rosenlof, 2012: A multidiagnostic intercomparison of tropical-width time series using reanalyses and satellite observations. *J. Climate*, **25**, 1061–1078, https://doi.org/10.1175/JCLI-D-11-00127.1.

Dee, D., and Coauthors, 2011: The ERA-Interim reanalysis: Configuration and performance of the data assimilation system. *Quart. J. Roy. Meteor. Soc.*, **137**, 553–597, https://doi.org/10.1002/qj.828.

Eyring, V., and Coauthors, 2013: Long-term ozone changes and associated climate impacts in CMIP5 simulations. *J. Geophys. Res. Atmos.*, **118**, 5029–5060, https://doi.org/10.1002/jgrd.50316.

Frierson, D. M. W., J. Lu, and G. Chen, 2007: Width of the Hadley cell in simple and comprehensive general circulation models. *Geophys. Res. Lett.*, **34**, L18804, https://doi.org/10.1029/2007GL031115.

Garfinkel, C. I., D. W. Waugh, and L. M. Polvani, 2015: Recent Hadley cell expansion: The role of internal atmospheric variability in reconciling modeled and observed trends. *Geophys. Res. Lett.*, **42**, 10 824–10 831, https://doi.org/10.1002/2015GL066942.

Gelaro, R., and Coauthors, 2017: The Modern-Era Retrospective Analysis for Research and Applications, version 2 (MERRA-2). *J. Climate*, **30**, 5419–5454, https://doi.org/10.1175/JCLI-D-16-0758.1.

Gillett, N. P., J. C. Fyfe, and D. E. Parker, 2013: Attribution of observed sea level pressure trends to greenhouse gas, aerosol, and ozone changes. *Geophys. Res. Lett.*, **40**, 2302–2306, https://doi.org/10.1002/grl.50500.

GISTEMP Team, 2016: GISS Surface Temperature Analysis (GISTEMP). NASA Goddard Institute for Space Studies, accessed 18 January 2017, https://data.giss.nasa.gov/gistemp.

Hansen, J., R. Ruedy, M. Sato, and K. Lo, 2010: Global surface temperature change. *Rev. Geophys.*, **48**, RG4004, https://doi.org/10.1029/2010RG000345.

Harrington, L. J., D. J. Frame, E. M. Fischer, E. Hawkins, M. Joshi, and C. D. Jones, 2016: Poorest countries experience earlier anthropogenic emergence of daily temperature extremes. *Environ. Res. Lett.*, **11**, 055007, https://doi.org/10.1088/1748-9326/11/5/055007.

Hawkins, E., and R. Sutton, 2012: Time of emergence of climate signals. *Geophys. Res. Lett.*, **39**, L01702, https://doi.org/10.1029/2011GL050087.

Hu, Y., and Q. Fu, 2007: Observed poleward expansion of the Hadley circulation since 1979. *Atmos. Chem. Phys.*, **7**, 5229–5236, https://doi.org/10.5194/acp-7-5229-2007.

——, L. Tao, and J. Liu, 2013: Poleward expansion of the Hadley circulation in CMIP5 simulations. *Adv. Atmos. Sci.*, **30**, 790–795, https://doi.org/10.1007/s00376-012-2187-4.

Hurrell, J. W., J. J. Hack, D. Shea, J. M. Caron, and J. Rosinski, 2008: A new sea surface temperature and sea ice boundary dataset for the Community Atmosphere Model. *J. Climate*, **21**, 5145–5153, https://doi.org/10.1175/2008JCLI2292.1.

IPCC, 2013: *Climate Change 2013: The Physical Science Basis.* Cambridge University Press, 1535 pp., https://doi.org/10.1017/CBO9781107415324.

Johanson, C. M., and Q. Fu, 2009: Hadley cell widening: Model simulations versus observations. *J. Climate*, **22**, 2713–2725, https://doi.org/10.1175/2008JCLI2620.1.

Kang, S. M., and J. Lu, 2012: Expansion of the Hadley cell under global warming: Winter versus summer. *J. Climate*, **25**, 8387–8393, https://doi.org/10.1175/JCLI-D-12-00323.1.

Kay, J. E., and Coauthors, 2015: The Community Earth System Model (CESM) Large Ensemble Project: A community resource for studying climate change in the presence of internal climate variability. *Bull. Amer. Meteor. Soc.*, **96**, 1333–1349, https://doi.org/10.1175/BAMS-D-13-00255.1.

Keller, K. M., F. Joos, and C. Raible, 2014: Time of emergence of trends in ocean biogeochemistry. *Biogeosciences*, **11**, 3647–3659, https://doi.org/10.5194/bg-11-3647-2014.

Kobayashi, S., and Coauthors, 2015: The JRA-55 Reanalysis: General specifications and basic characteristics. *J. Meteor. Soc. Japan*, **93**, 5–48, https://doi.org/10.2151/jmsj.2015-001.

Kushner, P. J., and Coauthors, 2018: Canadian snow and sea ice: Assessment of snow, sea ice, and related climate processes in Canada's Earth system model and climate-prediction system. *Cryosphere*, **12**, 1137–1156, https://doi.org/10.5194/tc-12-1137-2018.

Lehner, F., C. Deser, and L. Terray, 2017: Toward a new estimate of "time of emergence" of anthropogenic warming: Insights from dynamical adjustment and a large initial-condition model ensemble. *J. Climate*, **30**, 7739–7756, https://doi.org/10.1175/JCLI-D-16-0792.1.

Liebmann, B., R. M. Dole, C. Jones, I. Bladé, and D. Allured, 2010: Influence of choice of time period on global surface temperature trend estimates. *Bull. Amer. Meteor. Soc.*, **91**, 1485–1491, https://doi.org/10.1175/2010BAMS3030.1.

Lu, J., G. A. Vecchi, and T. Reichler, 2007: Expansion of the Hadley cell under global warming. *Geophys. Res. Lett.*, **34**, L06805, https://doi.org/10.1029/2006GL028443; Corrigendum, **34**, L14808, https://doi.org/10.1029/2007GL030931.

Lucas, C., B. Timbal, and H. Nguyen, 2014: The expanding tropics: A critical assessment of the observational and modelling studies. *Wiley Interdiscip. Rev.: Climate Change*, **5**, 89–112, https://doi.org/10.1002/wcc.251.

Lyu, K., X. Zhang, J. A. Church, and J. Hu, 2015: Quantifying internally generated and externally forced climate signals at regional scales in CMIP5 models. *Geophys. Res. Lett.*, **42**, 9394–9403, https://doi.org/10.1002/2015GL065508.

Orlowsky, B., and S. I. Seneviratne, 2013: Elusive drought: Uncertainty in observed trends and short- and long-term CMIP5 projections. *Hydrol. Earth Syst. Sci.*, **17**, 1765–1781, https://doi.org/10.5194/hess-17-1765-2013.

Quan, X.-W., M. P. Hoerling, J. Perlwitz, H. F. Diaz, and T. Xu, 2014: How fast are the tropics expanding? *J. Climate*, **27**, 1999–2013, https://doi.org/10.1175/JCLI-D-13-00287.1.

Rienecker, M. M., and Coauthors, 2011: MERRA: NASA's Modern-Era Retrospective Analysis for Research and Applications. *J. Climate*, **24**, 3624–3648, https://doi.org/10.1175/JCLI-D-11-00015.1.

Scherer, M., and N. S. Diffenbaugh, 2014: Transient twenty-first century changes in daily-scale temperature extremes in the United States. *Climate Dyn.*, **42**, 1383–1404, https://doi.org/10.1007/s00382-013-1829-2.

Seidel, D. J., and W. J. Randel, 2007: Recent widening of the tropical belt: Evidence from tropopause observations. *J. Geophys. Res.*, **112**, D20113, https://doi.org/10.1029/2007JD008861.

Seviour, W. J. M., S. M. Davis, K. M. Grise, and D. W. Waugh, 2018: Large uncertainty in the relative rates of dynamical and hydrological tropical expansion. *Geophys. Res. Lett.*, **45**, 1106–1113, https://doi.org/10.1002/2017GL076335.

Sigmond, M., and J. C. Fyfe, 2016: Tropical Pacific impacts on cooling North American winters. *Nat. Climate Change*, **6**, 970–974, https://doi.org/10.1038/nclimate3069.

Son, S.-W., S.-Y. Kim, and S.-K. Min, 2018: Widening of the Hadley cell from Last Glacial Maximum to future climate. *J. Climate*, **31**, 267–281, https://doi.org/10.1175/JCLI-D-17-0328.1.

Taylor, K. E., R. J. Stouffer, and G. A. Meehl, 2012: An overview of CMIP5 and the experiment design. *Bull. Amer. Meteor. Soc.*, **93**, 485–498, https://doi.org/10.1175/BAMS-D-11-00094.1.

Vallis, G. K., P. Zurita-Gotor, C. Cairns, and J. Kidston, 2015: Response of the large-scale structure of the atmosphere to global warming. *Quart. J. Roy. Meteor. Soc.*, **141**, 1479–1501, https://doi.org/10.1002/qj.2456.

Wuebbles, D. J., and Coauthors, 2017: Climate science special report: Fourth national climate assessment. D. J. Wuebbles et al., Eds., U. S. Global Change Research Program Rep., Vol. 1, 470 pp., https://doi.org/10.7930/J0J964J6.